National Technical University of Athens
School of Civil Engineering
Laboratory of Earthquake Engineering

FRAGILITY ASSESMENT OF OFFSHORE WIND TURBINES SUBJECTED TO EXTREME SEA STATES

Submitted in partial fulfillment of the requirements
for the degree of MSc in Analysis and Design
of Earthquake Resistant Structures

Achilleas Anagnostou

October 2022

Supervisor: Dr. Michalis Fragiadakis, Associate Professor NTUA

Acknowledgments

I would like to thank my supervisor, Associate Prof. Michalis Fragiadakis, for the support and the encouragement he provided during this study. His friendly guidance and his insight made this work possible.

I would also like to express my gratitude to my parents, siblings and friends for continuously supporting me throughout my studies.

Abstract

Wind energy plays an important role in mitigating the adverse effects that fossil fuel produced power has on the environment. This has led to a rapid growth of the wind energy market during the last few decades. Concerning wind energy, onshore wind is generally preferable to offshore, primarily due to the increased construction costs associated with the latter. However, offshore wind farms have the capacity to generate more energy than their onshore counterparts. Increase of the economic efficiency of offshore wind turbines can be achieved by assessing their structural reliability.

Offshore wind turbines are subjected to a number of natural hazards all of which are random in nature. Among these, hydrodynamic loads due to wind generated waves are often dominant. The most common method for quantifying these loads is the use of linear wave theory to model regular extreme waves with a specified return period (e.g., 100-year). The hydrodynamic loads can be represented by their static equivalents. However, it is known that higher order non-linear terms have a significant effect on the produced wave-induced loads, especially in shallow waters where offshore wind turbines are often situated. Furthermore, irregular waves, i.e., waves produced by summing many regular waves with different frequencies indicated by a wave power spectrum describing a particular sea state, offer a more accurate representation of sea waves.

Assessing the vulnerability of an offshore wind turbine's support structure to natural hazards can be achieved by performing fragility analysis. This framework is traditionally used in earthquake engineering; however, the same philosophy has been followed to investigate the fragility of offshore wind turbines subjected to environmental hazards.

This study investigates the fragility of an offshore wind turbine fixed to the sea bed as a function of increasingly intense sea states. Wind and wave loads are imposed on the turbine's support structure. Environmental conditions present at a particular site located in west France are considered when calculating the loads. Irregular nonlinear waves are simulated using Pierson-Moskowitz (PM) wave power spectra to represent the sea states considered, while the hydrodynamic loads are obtained using Morison's equation. For simplicity, wind loads are considered to be static and are determined assuming extreme wind conditions on site regardless of the intensity of the sea state investigated.

The significant wave height is used as the sea state intensity measure, ranging from 1 to 40 m. The fragility curves produced refer to three damage limit states defined after performing a pushover analysis for the wind turbine. The first corresponds to 50% of the drift at the peak at which yielding of the structure occurs, the second corresponds to the yielding displacement and the third to the drift at the peak at which maximum capacity is obtained. Extreme responses of the structure obtained by implementing dynamic nonlinear analyses were used to determine whether a particular damage state has been attained, while the exceedance probability for each damage state was estimated using the Monte Carlo simulation method.

Contents

1. Introduction to Offshore Wind Turbines

1.1. Introduction

Wind power is a form of energy which has been used by humans for centuries. Wind is caused by the Sun's uneven heating of the Earth's surface, while the direction the wind is blowing is determined by the Earth's rotation and the topography of the land [1]. Initially, wind power was mainly used to grind grain and to pump water. Denmark, the United States and Scotland pioneered the production of the first electricity generating wind machines during the 19th century [2]. However, the use of wind to generate electricity quickly fell out of favor as grid electricity derived from fossil fuels was supplied to rural areas.

The past several years, as the effects of climate change have become more profound, the need for reduction of greenhouse gas emissions and the transition from fossil fuel power to more sustainable forms of energy, has led to a rapid growth of the renewable energy market. Overall, from 2012 to 2020, renewables reached 83% of net power capacity additions, with solar PV (around 139 GW added) and wind (93 GW added) making up the bulk of those additions [3]. In Europe there was 17.4 GW of new wind power capacity installation in 2021 adding to a total of 236 GW. UK installed the most wind power capacity in 2021 (2.6 GW), while 88% of that was offshore wind [4].

Even though the last few years there has been a growing interest in offshore wind, its share in the total gross power generation is still low, mainly due to the significantly higher costs associated with it. Comparing the costs of power produced by utilizing different technologies, can be achieved by determining the Levelized Cost Of Electricity (LCOE) associated with each one. LCOE is the total cost to build and operate a power-generating asset over the amount of power produced throughout its service life [5].

Despite the high LCOE of offshore wind turbines, there are those who believe that the future of wind energy lies offshore. When comparing offshore to onshore wind energy, it can be concluded that there are several advantages associated with the former. Wind speeds are higher and winds are generally more constant in offshore locations. Since the

power generated by a wind turbine is proportional to the cube of the wind velocity, offshore wind turbines have the potential to generate more electricity at a steadier rate. Additionally, electricity produced offshore could have lower transmission costs considering that most cities are situated in coastal regions close to potential offshore wind farm sites. Offshore wind turbines also face fewer challenges in terms of public acceptance than their onshore counterparts do.

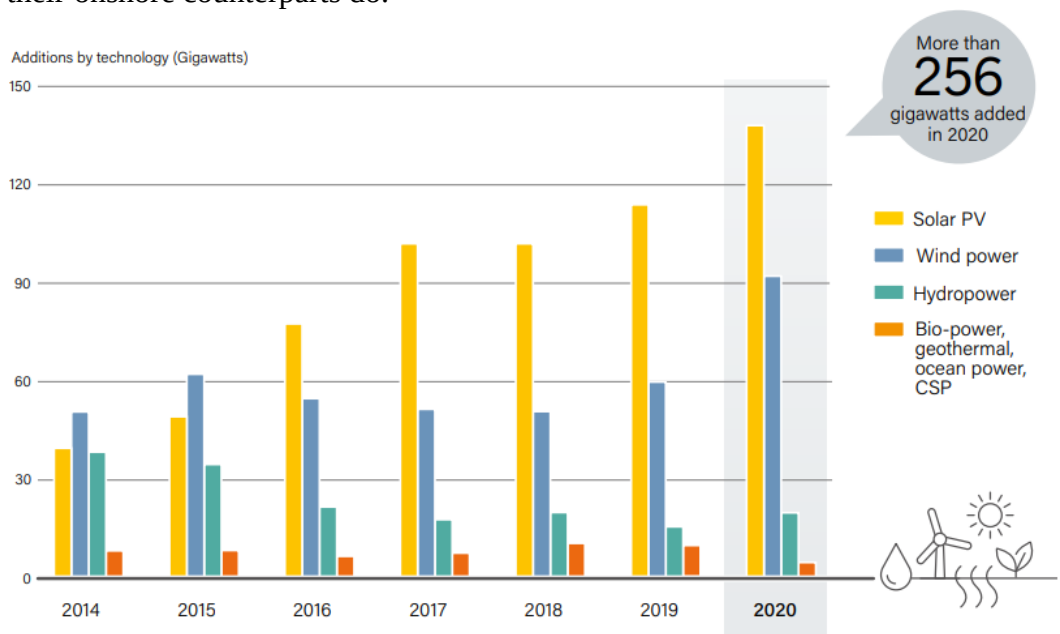

Fig. 1.1. Annual Additions of Renewable Power Capacity in Europe, by Technology and Total, 2014-2020 [4].

Reduction of the LCOE associated with offshore wind turbines during the coming years will play a key role in determining whether the offshore wind market will continue to grow. To achieve this, continuous technological improvements and innovation is required. Attempts to lower the LCOE and increase the efficiency of offshore wind farms the past years have led to larger wind turbines with higher rated power capacities. Today, 10 MW wind turbines are being developed and there are plans for the development of 20 MW turbines [1]. However, as the wind turbines upscale so do the required structures to support them.

Since the support structure of an offshore wind turbine accounts for a significant part of its overall cost, implementing structural optimization with respect to cost when designing it can be critical when assessing the wind turbine's economic feasibility [6]. To

achieve this, the reliability levels of the structure should be assessed. Considering that offshore wind turbines are subjected to a number of natural hazards all of which are random in nature, probabilistic analyses based on time-domain simulations can be a useful tool for performing an accurate reliability assessment.

1.2. Wind generated energy: Advantages and challenges

1.2.1. Advantages of wind generated energy

Although generating electricity using wind turbines is advantageous in many ways, the driving force behind the rapid growth of the wind energy sector the past years has been the need to shift from energy derived from the burning of fossil fuels, to cleaner and more sustainable types of energy. In that respect, wind is an excellent source of energy. Unlike power stations that use coal or oil, both of which are expendable, wind turbines can generate energy whenever the wind blows. Additionally, the electricity generated has zero carbon dioxide and sulfur dioxide emissions associated with it - the latter of which is largely responsible for acid rain - and is free of particulates which have been linked to the rise of diseases such as asthma and possibly Alzheimer's disease. Overall wind energy is associated with a relatively low amount of greenhouse gas emissions, which are attributed to the manufacture and transportation of the turbines and the blades.

There are other ways by which wind energy has less of an adverse impact on the environment when compared to other forms of energy. In contrast to fossil fuel derived power or nuclear power, both of which require the usage of large volumes of water, water is not used when harnessing wind to generate electricity. In addition, mining or pumping for resources, activities which are destructive to the environment, are not required for the operation of a wind turbine.

Apart from environmental reasons, the development of wind energy has had a stimulating effect on the economy as well. The past several years thousands of jobs have been created in the manufacturing, transportation, installation, servicing and working of wind turbines. Every year the cost of wind produced electricity decreases, as turbines become more efficient and are mass produced. Today the cost of wind produced electricity is very competitive with fossil fuel-derived electricity, while it is estimated that the cost of developing a wind turbine is recouped in the 7 months of its operation. Additionally, the cost of electricity produced by harnessing wind should be stable and should not vary with the price of imported fuels, which depends upon price hikes or potential embargoes.

Wind generated electricity has lower transport costs associated with it as well. Considering that wind farms are distributed across the land and are generally closer to cities in relation to fossil fuel power stations, the costs for transporting electricity (cables, pylons, loss of power due to electrical resistance) are lower. The selection of an appropriate site for the installation of a wind turbine is conditional only upon the site being windy. Such sites are often not in competition with urban development. Moreover, the same land can be used for other activities. For example, wind turbines can be erected on existing farms with little disturbance on general farming activities, while the land owner can make a profit from leasing his land to the electricity supply companies [1].

1.2.2. Challenges of wind generated energy

Despite the fast rate with which the wind industry has been growing the past 40 years, there are a lot of challenges when it comes to producing electricity using wind turbines. Arguably the greatest challenge associated with harnessing wind to produce electricity is the fact that wind does not always blow. This unpredictability of wind means that oftentimes wind farms may not be able to produce electricity due to a lack of wind in the area, or produce power at times when electricity is not required. To solve this problem, excess wind generated electricity needs to be stored and then used in times of need. Electricity can be stored in batteries, pumped water storage or by other means.

Since the ability of a wind turbine to generate electricity completely depends upon the wind blowing, the selection of a suitable site for a wind farm is of great importance. That being said, sites where higher wind speeds and more steady winds are reported are often in remote locations. Consequently, the power produced by wind farms situated at these sites has higher transportation costs when reaching consumers. Additionally, there are many arguments regarding the aesthetics of wind turbines and many believe that installing turbines in mountainous areas, where wind speeds are higher, takes a toll on the natural beauty of the location.

Regardless of the opinion one has about the appearance of wind turbines, there is no doubt that they generate a lot of noise when operating. Although the noise falls off exponentially with distance from the tower, noise pollution from operating wind turbines can become a challenge. This problem becomes greater when a wind farm is closer to urban areas, while as mentioned above, choosing sites further away from urban areas increases transportation costs.

Another reason why wind turbines should be installed away from human habitation is safety. The collapse of a wind turbine's supporting structure or one of its blades coming adrift can cause serious damage and is a major safety concern for people and animals nearby. Even when a wind turbine is operating normally, there is a lot of evidence that its blades can damage wildlife. It is estimated that in the US, 33,000 bird deaths a year are caused by the turning blades of wind turbines [1].

1.3. Wind turbines

Humans have been using wind power from 5000 BC to propel boats on the Nile River [7]. Machines able to harvest wind energy and convert it into mechanical energy existed in Egypt, Persia, Mesopotamia and China. Machines called windmills, referring to the process of grinding or milling grain such as wheat or corn utilizing the power of wind, is believed to have first appeared eastern Iran during the 9th century AD [8]. For over 1200 years windmills and water-driven mills were the only machines humans used to generate power.

During the 2nd world war, Denmark built a significant number of wind turbines with two and three blades so much so that the three bladed wind turbine design is usually called the classical Danish concept. Today, as fossil fuels are becoming less available and concerns related to pollution and climate change increase, wind energy conversion is being reinvented, as has happened many times over the years, integrating new materials and technologies.

1.3.1. Types of wind turbines

There are two types of wind turbines that are developed today. These are the horizontal axis turbines (HAWTs) which rotate about the horizontal axis parallel to the ground and the vertical axis turbines (VAWTs) which rotate about the vertical axis perpendicular to the ground. Historically, the first known wind turbines had been VAWTs although HAWTs are generally more efficient and are the most common turbines used today.

A number of researches employing the fragility analysis method to offshore wind turbines can be found in the literature.

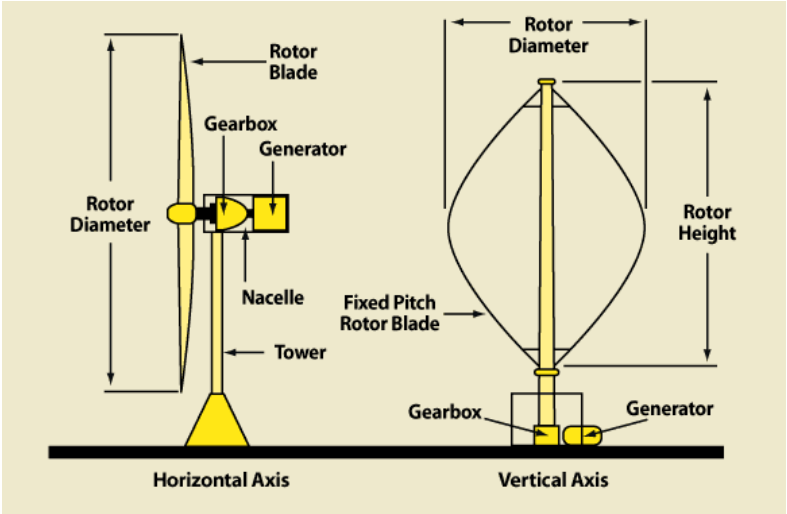

Fig. 1.2. Types of wind turbines [9].

1.3.1.1. Vertical Axis Wind Turbines

The first wind turbines used by humans were VAWTs. As early as the 7th century BC, vertical-axis wind machines were used in Babylon with the purpose of irrigating the fertile plains of the Eyphrates and Tigris Rivers [10]. Their main advantage compared to HAWTs is that they are omnidirectional, that is they can produce power from wind blowing from every direction. VAWTs also have the capacity for the gearbox and other equipment to be placed closer to the ground, since the turbine's orientation is vertical, which reduces maintenance costs. The two most known types of VAWTs are usually called the Darrieus VAWT and the Savonius VAWT, in honor of the engineers who first patented them, Georges Jean Marie Darrieus [11] and Sigurd Johannes Savonius [12], respectively.

The Savonius VAWT was first patented in 1925. Rotation of the blades occurs due to unequal amounts of drag of the blades. However, these types of VAWTs only produce torque suitable for generating power only when the blade is moving in the same direction the wind is blowing. As a result, power can only be gained during one half of the blade revolution. A more efficient type of VAWT is the Darrieus VAWT which is based on the concept of aerodynamic lift to harness the wind and produce torque in the gearbox. Darrieus VAWTs utilize blades made of airfoils and are able to achieve power production during the full revolution of the blade. An example of a Darrieus VAWT is shown schematically in Fig. 1.2.

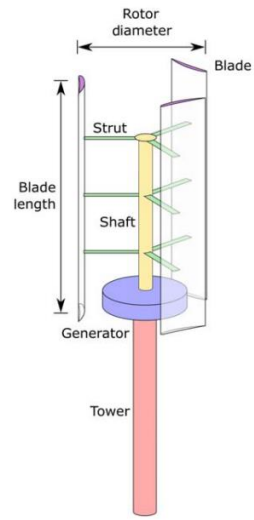

Fig. 1.3. Schematic of a modern lift-based Vertical Axis Wind Turbine (VAWT) [1].

1.3.1.2. Horizontal Axis Wind Turbines

Horizontal axis windmills appeared in western Europe between 1300 and 1975 AD [7]. The blades of a HAWT rotate due to aerodynamic lift forces, perpendicular to the direction of wind flow. The mechanics are very much similar to those involved in aviation. HAWTs are more efficient than VAWTs, however, since the axis of a HAWT must be facing the wind for aerodynamic lift to appear in the turbine's blades, the turbine must yaw to account for changes in wind direction. Consequently, wind conditions which reduce the number of instances a HAWT must yaw, such as those encountered in sites with low turbulence and consistent winds, are more suitable for HAWTs.

Even though HAWTs can have any number of blades, the addition of blades leads to increased costs and reduction in the time each blade has before it encounters its wake. When the blades of an even bladed turbine are vertical, the wind forces acting on the blade which is at the top maximize, while forces acting on the blade which is at the bottom, and at that point is crossing in front of the pole of the tower, minimize. As a result, a HAWT with an even number of blades would require a hinged hub, able to tilt in order to avoid heavy shocks to the turbine and tower when the blades become vertical. The vast majority of wind turbines developed today have three blades, offering a balance between efficiency and structural stability [13].

Contemporary HAWTs are made up of three different parts:

- The first part is the aerodynamic rotor of the wind turbine, which consists of the hub and the blades. The blades are attached to the hub and are responsible for the conversion of wind energy to kinetic mechanical energy.
- The second part consists of the mechanical and electrical parts, which are housed at the top of the wind turbine inside the nacelle, and are responsible for turning the kinetic mechanical energy to electricity.
- The third part of the wind turbine is its structural support which is made up of the wind turbine foundation, the substructure and tower.

The parts comprising a modern HAWT are shown in Fig. 1.4.

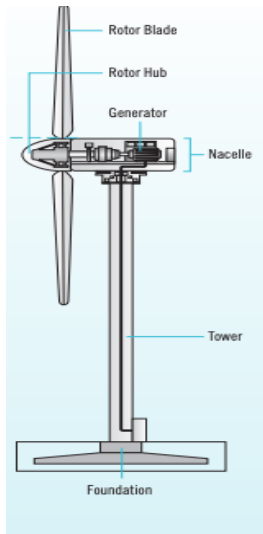

Fig. 1.4. Schematic of a modern Horizontal Axis Wind Turbine (HAWT) [14].

1.4. Offshore wind

It is true that there is a lot more onshore wind energy produced today than offshore wind energy. Principally, the popularity of onshore wind energy has to do with cost. Although offshore wind energy is associated with large initial capital investments and longer construction times [15], there is a growing interest for the construction of more offshore wind farms, especially in the developing countries [16]. While the few existing

offshore wind farms are located in shallow waters, there are plans for the construction of very large wind farms in deep waters.

This growing interest in offshore wind is for the most part attributed to the wind conditions which are present at sea. As was already illustrated in this paper, wind speed plays a major role when determining the power a wind turbine can produce. While wind speed varies significantly across different geographical regions, it is true that offshore locations are characterized by higher and more consistent wind speeds. As a result, offshore wind farms have the potential to produce more electrical power and at a steadier rate than onshore wind farms [17].

Although the effect offshore wind farms have on the oceanic environment is not yet fully understood, there is evidence that onshore wind farms have more of an adverse environmental and health impact than their offshore counterparts [18]. It is very common for groups of people living in areas close to onshore wind farms to express concerns about the effects of noise pollution introduced by the wind farm's operation on their lives and the surrounding environment. In contrast, Offshore wind farms which are located far out at sea tend to generate far less complaints about their construction [16].

Offshore wind does have its disadvantages though. As already mentioned, the biggest one of them is the cost. Offshore wind farms are hard to reach resulting in higher building and maintenance costs. Adding to the cost associated with them is the infrastructure required for them to connect to the grid (e.g., underwater cable connections). Offshore wind turbines are also exposed to rougher environments than onshore turbines do. High wind speeds and wave heights, for example during a storm or a hurricane, make it more probable the wind turbine will sustain damage. Despite these shortcomings, as technology keeps improving, it is likely that in the future offshore wind farms will become as cheap as their onshore counterparts [17]

2. Benchmark Offshore Wind Turbine and environmental loads

An offshore wind turbine's (OWT) support structure is affected by the environment in a number of ways, while some of them have more of a profound effect on it than others. Predominantly, the environmental loads an OWT is subjected to originate from waves, current and the wind, while among those, wind-induced wave loads are often the most dominant [19]. Since all environmental loads are random in nature, designing such structures is always associated with some amount of uncertainty. Attempting to quantify wave induced loads on a fixed offshore structure for example, entails the use of statistical met-ocean data for a specific region, namely, the wave height (H) and the wave period (T). Assessing the safety of a structure subjected to such loads, while still taking into account the uncertainties introduced when quantifying them, can be achieved by determining the structure's probability of failure (p_f).

Conventionally, methods for designing offshore structures are based on checking whether they can withstand environmental loads with a specified return period (e.g., 100-year). The most straightforward way of doing that is by modeling regular extreme waves using a linear wave theory. The hydrodynamic loads can be represented by their static equivalents [22]. However, it has been shown that the contribution of higher order nonlinear terms to wave-induced loads is significant, especially in shallow waters where OWTs are generally situated, due to the non-linearity exhibited by the drag component [23]. Moreover, a more realistic representation of sea waves can be achieved if they are modelled as irregular, i.e., as a sum of many waves with different frequencies within a range indicated by a wave power spectrum describing a particular sea state. The hydrodynamic loads can then be obtained after calculating the wave kinematics in the time domain. Other uncertainties regarding the extreme responses of structures subjected to irregular wave-induced loads, like structural dynamics effects or material properties, can be taken into account if a probabilistic reliability approach is implemented [25].

2.1. Benchmark Offshore Wind Turbine considered

The Vestas V90-3MW OWT is examined in this study. The wind turbine is three bladed with an upwind oriented rotor and a wind speed rating of 15 m/s. The hub stands at a height of 92 m above water, while the water depth is 33 m. Circular hollow sections comprise the wind turbine's support structure which has a total length of 125 m and it consists of the substructure and the tower. The substructure is 45 m long, with a diameter of 4 m and a thickness of 6.5 cm. The tower's length is 80 m, while its cross-section varies linearly with height, starting with a diameter of 4 m and a thickness of 6.5 cm at the point where it connects with the substructure, and ending with a diameter of 2.8 m and a thickness of 2 cm at the top. Information regarding the turbine's properties is listed in 0, while detailed information can be found in reference [26]. To allow for emphasis to be given to the impact increasingly intense sea states have on the fragility of the wind turbine, several simplifying assumptions were made. The monopile foundation of the wind turbine is assumed to be rigidly fixed to the seabed; the seabed is assumed to be flat; extreme wind loads are imposed statically and it is assumed that they act in the same direction as the hydrodynamic loads originating from waves. A schematic representation of the wind turbine is shown in 0.

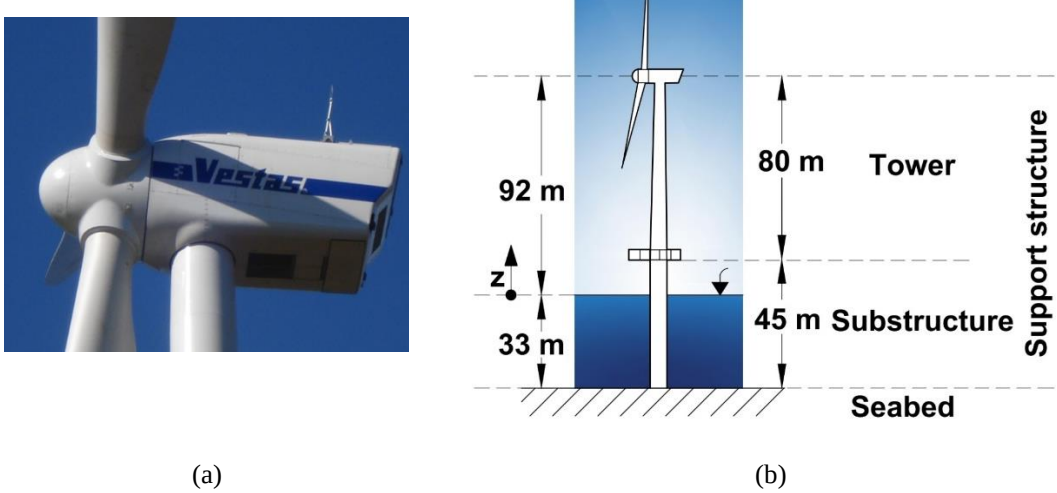

(a) (b)

Fig. 2.1 (a) Vestas V90 – 3 MW wind turbine; (b) schematic representation of the offshore wind turbine considered

Table 2.1 Properties of the Vestas V90-3MW offshore wind turbine [26].

Vestas V90-3MW	
Rated power	3,000 kW
Rotor orientation	Upwind
Number of blades	3
Rotor diameter	90 m
Nacelle weight	70,000 kg
Rotor weight	41,000 kg
Cut-in, rated, cut—out wind speed	3.5 m/s, 15 m/s, 25 m/s
Hub height	92 m
Water depth	33 m
Tower length	80 m
Substructure length	45 m
Tower base diameter, thickness	4 m, 0.065 m
Tower top diameter, thickness	2.8 m, 0.02 m
Substructure diameter, thickness	4 m, 0.065 m

The description of the environmental conditions essential for deriving the wind and wave loads is given by the "Marine Renewable Integrated Application Platform" or "MARINA – Platform" [27]. The conditions present at the SEM-REV sea test site, located in France (west coast), were used in this study. Parameters describing extreme environmental conditions which may occur at the referenced site are listed in 0. Specifically, for the description of the extreme sea state, two parameters are being used; the significant wave height, H_s, which is the average height between the trough and the crest of the highest one-third waves, and the spectral peak period, T_p, which is the period of oscillation of the most energetic waves, i.e., the period that corresponds to the peak of the wave power spectrum describing a particular sea state. Extreme wind conditions are described in terms of the mean wind speed at 10-meter height above the mean sea water level, U_w.

Table 2.2 Extreme environmental conditions present at the referenced site [27].

SEM-REV, France	
50-year U_w at 10m	23.76 m/s
50-year H_s	8.15 m
Mean value of T_p	11.06 s

A 3D beam element model of the wind turbine support structure is developed using OpenSeesPy library (version 3.4.0.1), a Python 3 interpreter of the OpenSees software [28]. A total of 125 force-based beam-column elements are used to model both the substructure and the tower, each with length 1 m. It is noted that this resolution for discretizing the support structure is adopted to account for the variability of the tower's tubular cross section as well

as to assist the modelling of the in-height distribution of the wave and wind loads. At the cross-sectional plane, each element is divided into 40 fibers in the circumferential direction and 40 fibers in the radial direction. Both material and geometrical non-linearity are being taken into account in the model. The material used for modeling the support structure is high strength steel with yield stress equal to 355 MPa and modulus of elasticity equal to 210 GPa. A bi-linear model with kinematic hardening is used for the material itself, while the ratio between the post-yield modulus and the initial modulus of elasticity is assumed to be equal to 1%. The mass of each element is assumed to be lumped at the nodes, while both the rotor and nacelle masses are lumped at the top node of the structure.

After the model is developed, modal analysis is performed using the OpenSees software. It is noted that due to axial symmetry, the produced eigenmodes concerning vibrations along the X and Y global axis come in pairs with same magnitude and eigenperiods. The resulting eigenperiods and modal mass participation for the first 8 eigenmodes are shown in 0, while the corresponding modes are presented in 0.

Table 2.3 Modal analysis of the wind turbine.

Eigenmode	Eigenperiod (sec)	Mass participation ratios (%)
T_1, T_2	3.90	47.01
T_3, T_4	0.85	23.38
T_5, T_6	0.30	10.06
T_7, T_8	0.15	5.15

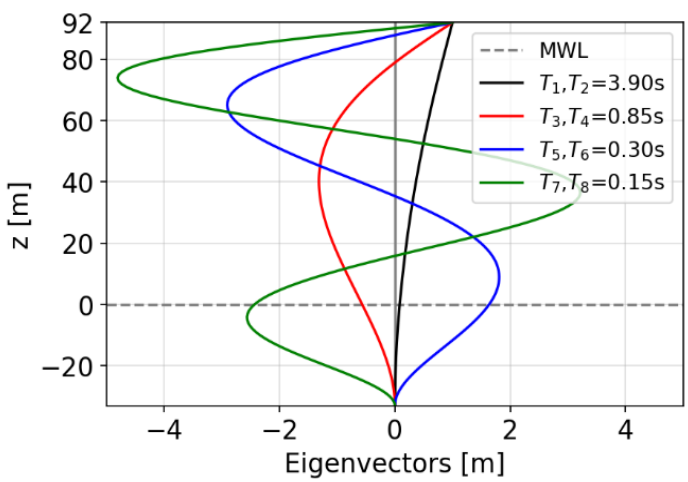

Fig. 2.2 Eigenmodes of the OWT's support structure.

2.2. Environmental loads

Two types of environmental loads are considered; wave loads and wind loads. A schematic representation of the applied loads can be seen in Fig. 2.3. The hydrodynamic wave loads are calculated by simulating irregular nonlinear wave kinematics using wave power spectra to represent increasingly intense sea states. The significant wave height (H_s) and the spectral peak period (T_p) are the two parameters used for defining each wave spectrum, the former being the measure with which the intensity of the sea state is indicated. For simplicity, wind loads are considered to be static, acting above the mean sea water level, along the height of the structure. Regardless of the intensity of the sea state investigated, the wind loads are determined assuming extreme wind conditions on site.

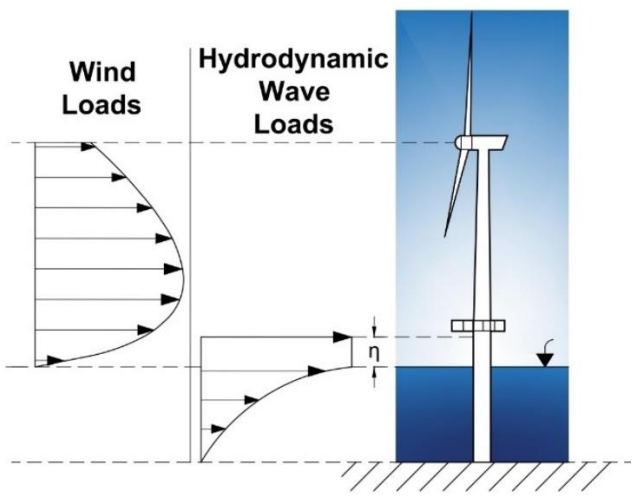

Fig. 2.3 Loads applied to benchmark OWT.

2.2.1. Wind loads along the height of the wind turbine

The technical rules and guidance regarding the calculation of the wind loads applied to the wind turbine can be found in Eurocode 1 [29]. The fundamental value of the basic wind velocity, $v_{b,0}$ is taken equal to 23.76 m/s, which is the mean wind speed at a height 10 m above ground (U_w), associated with a 50-year return period for the site considered [27]. The mean wind speed $v_m(z)$ at a height z above the water level is obtained as:

(1)

$$v_m(z) = c_r(z) \cdot c_0 \cdot v_b \tag{2.1}$$

where v_b is the basic wind velocity, c_0 is the orography factor and $c_r(z)$ is the terrain roughness factor. v_b depends on the directional and season factors, which are considered equal to 1, and thus v_b is equal to $v_{b,0}$. The variation along the height z of the wind turbine's support structure is accounted by the terrain roughness factor and is based on a logarithmic velocity profile $c_r(z) = k_r \cdot \ln(z/z_0)$. The wind forces that act on the wind turbine are calculated as a summation over the 1 m length cylindrical elements of the structure using the expression:

$$F_w = c_s c_d \sum_{elements} c_f \cdot q_p(z_e) \cdot A_{ref} \tag{2.2}$$

where $c_s c_d$ is the structural factor, c_f is the force coefficient for cylindrical elements, $q_p(z_e)$ is the peak velocity profile at reference height z_e and A_{ref} is the reference area of the cylindrical elements. Following the detailed procedure given by [29] for calculating $c_s c_d$, the structural factor is determined to be equal to 1.07. The profile of the wind loads for the case study OWT, along the height of the turbine are shown in 0. The profile has a parabolic shape that receives its maximum volume for z = 40m.

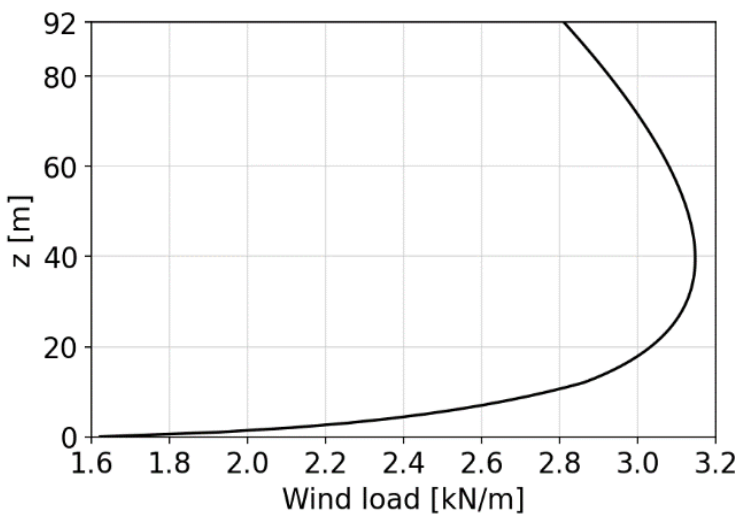

Fig. 2.4 Wind loads along the height of the wind turbine.

2.2.2. Hydrodynamic wave induced loads

The support structure of the OWT is subjected to loads induced by non-linear uni-directional waves characterized by significant wave heights (H_s) that range from 1 to 40 m. Due to their large variability, the wave loads are treated as stochastic variables. To capture the randomness of the loads, random (irregular) wave kinematics should be simulated. This can be achieved by summing the kinematics of a number of regular wavelets each associated with a distinct period – or frequency – of oscillation. A random phase angle is assigned to each wavelet introducing thus the randomness sought in the produced irregular wave. Furthermore, the amplitude of these wavelets is considered to be a random variable which depends upon a two-parameter wave power spectrum characterizing a particular sea state. The power spectrum also indicates the range of values for the distinct frequencies of oscillation associated with each wavelet considered. In that sense, frequencies which appear to be correlated with extremely low energy need not be taken into account while only the range of frequencies within which the magnitude of energy is high should be included.

The spectral peak period (T_p) is used as a second parameter along with the significant wave height (H_s) in order to produce the wave power spectra that characterize the different sea states. Regarding the site considered [27], the spectral peak period (T_p) follows a lognormal distribution conditional on wind speed at a height 10 m above water (U_w) and on the significant wave height (H_s). Since U_w is already considered to be equal to 23.76 m/s, the values for T_p are calculated using Eq. 2.3 as the mean value of all the possible values it would take for each value of H_s considered.

$$T_p(H_s,U_w) = \overline{T_p}(H_s)\cdot\left[1-0.268\left(\frac{U_w-\bar{u}(H_s)}{\bar{u}(H_s)}\right)\right] \tag{2.3}$$

where $\overline{T_p}(H_s)$ and $\bar{u}(H_s)$ are the expected spectral peak period and the mean wind speed, respectively. $\overline{T_p}$ and $\bar{u}$ are expressed as functions of the significant wave height and are given by the expressions below:

$$\overline{T_p}(H_s) = 5+5.833\cdot H_s^{0.201} \tag{2.4}$$

$$\bar{u}(H_s) = 2+3.947\cdot H_s^{0.620} \tag{2.5}$$

The Pierson-Moskowitz (PM) power spectrum is used to simulate the different sea states. The irregular waves are modeled as a summation of 1000 wavelets over a range of frequencies indicated by the magnitude of energy within the PM spectrum. The definition of the PM spectrum is given by the DNV-RP-C205 guidelines [30] and is obtained as follows:

$$S_{PM}(\omega) = \frac{5}{16} H_s^2 \omega_p^4 \cdot \omega^{-5} \exp\left[-\frac{5}{4} \left(\frac{\omega}{\omega_p} \right)^{-4} \right] \tag{2.6}$$

where ω is the angular velocity of each wavelet, while $\omega_p=2\pi/T_p$ and S_{PM} are the spectral peak angular velocity and the PM wave energy spectrum for each simulated sea state, respectively. Using Eqs. 2.3 and 2.6 the power spectra for increasingly higher values of H_s can be produced. For each wave spectrum produced this way, the range of frequencies within which energy is present is identified. 1000 regular wavelets associated with a distinct frequency within that range are then produced. When producing these regular wavelets, either linear or nonlinear wave theory can be used. However, it is known that, especially in shallow waters, the nonlinearity of the simulated waves significantly influences the resulting wave loads [23]. On the grounds of this, a second-order term is added for each wavelet and the surface elevation profile of each irregular wave is obtained using Eq. 2.7, where $\eta(x,t)$ indicates the second order-surface elevation. $\eta_1(x,t)$ and $\eta_2(x,t)$ are the first and second order surface elevation components, respectively and can be determined using Eqs. 2.8 and 2.9.

$$\eta(x,t) = \eta_1(x,t) + \eta_2(x,t) \tag{2.7}$$

$$\eta_1(x,t) = \sum_{i=1}^{nw} A_i \cdot \cos\left(\omega_i t - k_i x - \varphi_i \right) \tag{2.8}$$

$$\eta_2(x,t) = \sum_{i=1}^{nw} A_i^2 \cdot \frac{\pi}{2\lambda_i} \cdot \frac{\cosh\left(k_i d\right)}{\sinh^3\left(k_i d\right)} \cdot \left(2 + \cosh\left[2\left(k_i d\right)\right]\right) \cdot \cos\left[2\left(\omega_i t - k_i x - \varphi_i\right)\right] \tag{2.9}$$

where nw is the number of wavelets taken into account, ω_i is the equally-spaced discrete angular frequency of the wavelet, k_i is the associated wave number, λ_i is the associated wavelength, d is the water depth, φ_i is a random phase angle which follows a uniform distribution in the range $[0,2\pi]$ and A_i is the wave amplitude. The wave number $k_i = 2\pi/\lambda_i$ can be obtained using the dispersion relationship [30]. The wave amplitudes of the wavelets are

determined using the wave energy spectrum. As is demonstrated in [31] in order for the randomness of the simulated wave to be maintained, the amplitudes should not be assumed to be deterministic but they should be considered as random variables instead. In this study it is assumed that the amplitudes follow the Rayleigh distribution with mean square value given by $E[A_i^2] = 2 \cdot S_{PM}(\omega_i) \cdot d\omega_i$ [30].

In order to better explain the impact of the second order term on the wave elevation profile, an example is considered for which a regular wave is simulated with an H_s = 10 m and T_p = 13.17 s. Simulating a regular wave is, in effect, equivalent to using a delta function spectrum, which is one with energy present at a single frequency to simulate an irregular wave [32]. The first and second order regular wave components, η_1 and η_2 respectively, and the second-order wave produced as the sum of those η, are shown in 0. As is observed, inclusion of the second order component η_2 results to steeper crests and wider troughs of the produced wave. It can be seen that the second-order wave is asymmetric with respect to the mean water level.

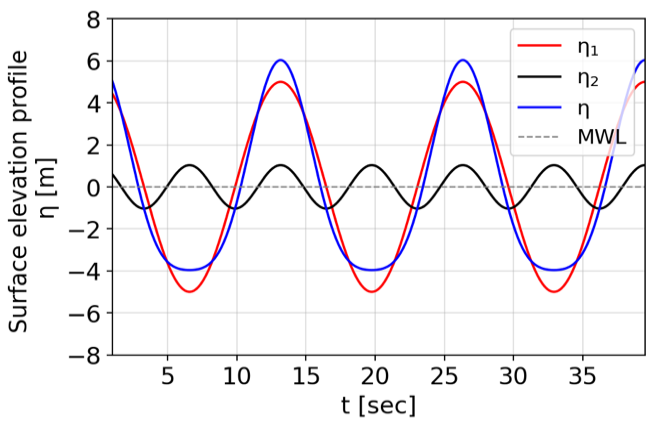

Fig. 2.5 Second order regular wave and its two wave components with H_s = 10 m and T_p = 13.17 s.

An example of the first 300 seconds of a simulated irregular wave elevation profile produced using the PM power spectrum is shown in 0. To validate the procedure for producing the surface elevation profile, the Fourier transform of 50 simulated waves is performed and the mean values are compared with the PM spectrum originally assumed (0). As shown in 0, the PM spectrum for a sea state characterized by an H_s = 10 m and T_p = 13.17 s indicates that energy is present for waves with frequencies of oscillation between approximately 0.25 and 1.75 rad/s.

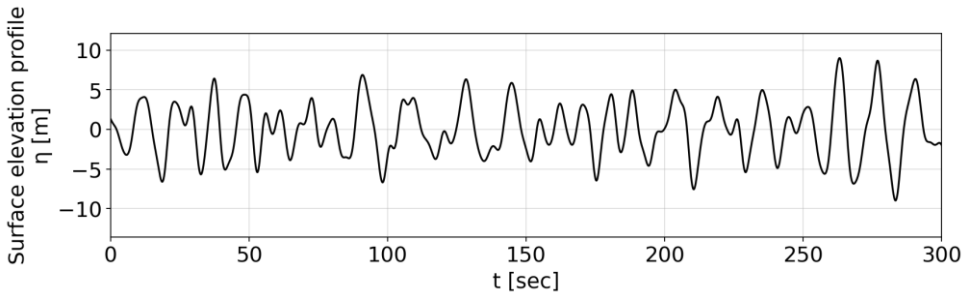

Fig. 2.6 Surface elevation profile of an irregular wave with H_s = 10 m and T_p = 13.17 s.

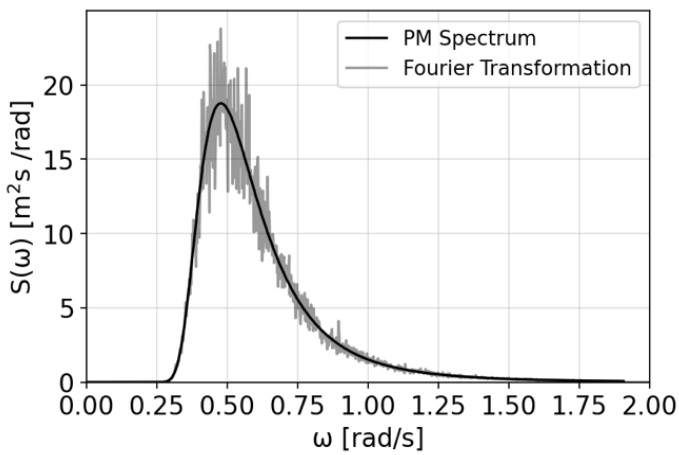

Fig. 2.7 PM spectrum and Fourier transformation of the surface elevation profile of 50 irregular waves with H_s = 10 m and T_p = 13.17s.

The wave induced horizontal hydrodynamic loads exerted on the submerged support structure are obtained using Morison's equation (Eq. 2.10) [30].

$$f_h(t) = \rho \cdot C_n \cdot A \cdot \dot{u} + \frac{1}{2} \cdot \rho \cdot C_d \cdot D \cdot u \cdot |u| \tag{2.10}$$

where ρ is the mass density of water, A is the cross-sectional area of the support structure, D is the diameter of the cross-section, $\dot{u}$ is the water particle acceleration and u is the water particle velocity. C_m and C_D are the inertia and drag coefficients and their evaluation is the critical aspect when calculating the hydrodynamic loads. Generally, both coefficients depend on the Reynolds number, the Keulegan-Carpenter number and the non-dimensional roughness. Experiments conducted at nominally the same conditions have shown that both

coefficients can vary considerably [33]. In this study C_m was taken equal to 1.20 and C_D equal to 1.05.

The water particle kinematics of the second order irregular wave are obtained by adding the kinematics of the two wave components. The horizontal particle velocity u and acceleration $\dot{u}$ of the first wave component are obtained using Eqs. 2.11 and 2.12 respectively, while Eqs. 2.13 and 2.14 are used to determine the kinematics of the second wave component [34].

$$u_1 = A_i \cdot \omega_i \cdot \frac{\cosh\left[k_i\left(d+z\right)\right]}{\sinh\left(k_i d\right)} \cdot \cos\left(k_i x - \omega_i t\right) \tag{2.11}$$

$$\dot{u}_1 = A_i \cdot \omega_i^2 \cdot \frac{\cosh\left[k_i\left(d+z\right)\right]}{\sinh\left(k_i d\right)} \cdot \sin\left(k_i x - \omega_i t\right) \tag{2.12}$$

$$u_2 = \frac{3}{4c_i} \cdot A_i^2 \cdot \omega_i^2 \cdot \frac{\cosh\left[2k_i\left(d+z\right)\right]}{\sinh^4\left(k_i d\right)} \cdot \cos\left[2\left(k_i x - \omega_i t\right)\right] \tag{2.13}$$

$$\dot{u}_2 = \frac{3\pi}{2\lambda_i} A_i^2 \cdot \omega_i^2 \cdot \frac{\cosh\left[2k_i\left(d+z\right)\right]}{\sinh^4\left(k_i d\right)} \cdot \sin\left[2\left(k_i x - \omega_i t\right)\right] \tag{2.14}$$

where c_i denotes the wavelet celerity. For the above equations, z takes values between 0 (mean water level) and $-d$. For positions above the mean water level, the water particle kinematics are obtained using the "vertical stretching" method due to its simplicity [20]. 0 shows the wave kinematics as well as the hydrodynamic loads for z = -33 m (seabed), z = -10 m and z = 0. The kinematics and the corresponding loads were produced by the irregular wave shown in 0. As shown in 0, the magnitude both of the kinematics and of the loads decrease the closer the current position gets to the seabed. This decrease of magnitude is more evident for the horizontal particle acceleration. Additionally, it is apparent that higher frequency wavelets have a greater impact on the resulting horizontal acceleration when compared to the horizontal velocity.

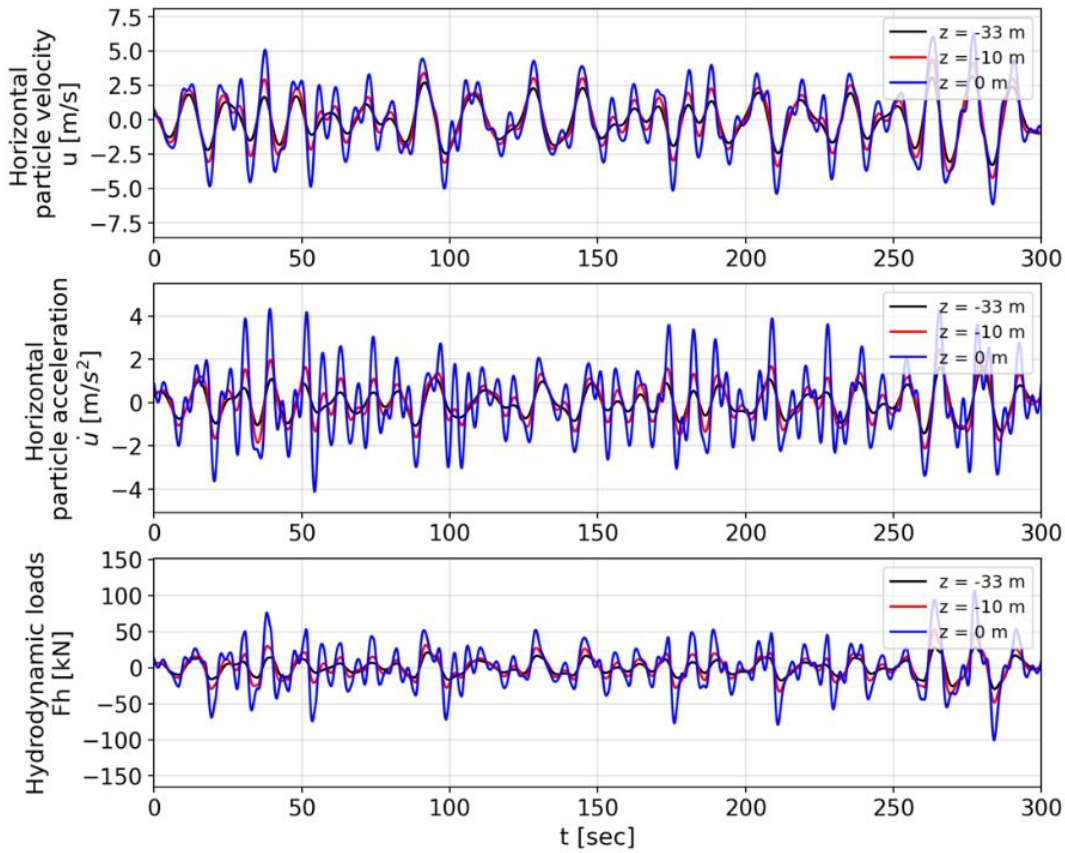

Fig. 2.8 Water particle kinematics and hydrodynamic loads along the sea depth due to an irregular wave with H_s = 10m and T_p = 13.17s.

3. Fragility Analysis of the Offshore Wind Turbine

Assessing the vulnerability of an OWT support structure to natural hazards like severe storms or earthquakes can be a useful tool for estimating costs associated with certain structural performance criteria. Fragility analysis is traditionally used in earthquake engineering to make such assessments, while numerous papers studying the fragility curves of frame buildings and bridges can be found in the literature [35]. Employing this method, a number of researchers have studied the seismic fragility of steel monopile wind turbine towers [39]. In recent years, the same philosophy has been followed to investigate the fragility of OWTs when subjected to environmental loads due to wind, wave and current. Wilkie and Galasso [42] propose a framework for quantifying financial losses associated with a monopile supported OWT exposed to extreme wind and wave loads, which involves the fragility assessment of the monopile as a function of mean wind speed and significant wave height. To achieve this, dynamic analyses were performed, while the sea-state assumed to be present was modelled as a random process and the resulting hydrodynamic loads were calculated using linear wave theory. Wei et al. [43] used probabilistic models for the structural demands to produce the fragility curves of an OWT with jacket-type support structure subjected to combined wind- and wave-induced loads for two damage states. To determine the wave loads, extreme wave heights associated with certain mean return periods were identified using non-linear irregular wave modeling and a JONSWAP wave spectrum. Mardfekri and Gardoni [44] developed probabilistic models to predict the structural demands of a monopile supported OWT and considered operational and environmental loads (wind, wave and current) when investigating its fragility, using wind speed and wave height as the intensity measures.

3.3. Fragility assessment

Performance-Based Engineering (PBE) combines computational tools and reliability assessment procedures in order to obtain the system fragility and risk for a range of limit-states. Conceptually, structural reliability provides a framework which incorporates the

uncertainties associated with environmental or structural loads, strength and stiffness. According to PBE, the acceptable level of damage depends on the intensity of a natural hazard and the significance of the structure considered. In this context, natural hazard intensities are represented by Intensity Measures (IM), while the demand - or the level of damage - is measured using Engineering Demand Parameters (EDP).

Fragility analysis requires the calculation of the probabilities that a number of monotonically increasing limit-states are exceeded. Therefore, the fragility F_R is defined as the limit-state probability conditioned on hazard intensity. These limit-states should represent certain Damage States (DS) the structure may attain. Whether or not a particular DS has been exceeded can be determined using a pertinent EDP. Therefore, the fragility of a system is the probability that an engineering demand parameter (EDP) exceeds a threshold value edp and is defined as:

$$F_R\left(IM, DS\right) = P\left(EDP \geq edp \mid IM\right) \tag{3.1}$$

In this study the drift at the top of the tower is used as the EDP and is obtained as the output of nonlinear dynamic analyses. Threshold values for the drift are defined, corresponding to certain performance criteria. The natural hazard considered are the wave induced loads. The IM selected for describing the hazard is the significant wave height H_s. For the purpose of investigating the performance of the OWT as function of the IM, 40 values for the H_s are considered scaling from 1 to 40 m. The step with which H_s is incremented is 1 m, i.e., $H_s^i = H_s^{i-1} + 1$. The exceedance probability of the predefined damage limit states for each IM is deduced by performing a number of Monte Carlo simulations. For each simulation the extreme drift at the top of the structure is used to evaluate whether a damage state has been attained.

3.4. Definition of damage states

In the present study the safety of the OWT is assessed with respect to three damage states. The criterion used for assessing whether the wind turbine has exceeded a particular damage state is the drift at the top of the tower. To identify the critical displacements, a static pushover analysis is carried out by incrementally controlling the horizontal displacement of the tip of the tower in the for-aft direction. A triangular distribution of loads is applied, increasing in magnitude from the bottom to the top of the OWT. The total vertical load corresponding to each displacement is obtained as the output of the analysis which was performed using the

OpenSees software. The produced curve representing the nonlinear drift at the top with increasing vertical loads is shown in 0. Two critical displacements considered by other researchers when investigating the fragility of OWTs are defined as 50% of the yielding displacement of the tower [45] and the displacement at which the yielding occurs [40] [46]. As can be observed in 0, a nonlinear relation between the displacement at the top and the vertical loads appears at a drift of about 1.92%, which is used as the critical yield drift defining the first two damage states (DS1 and DS2) adopted in this study, DS1 corresponding to 0.96% and DS2 corresponding to 1.92% drift at the top. The third damage state DS3 corresponds to the total damage (collapse) of the OWT and is considered to occur at a drift equal to 2.72% at which the pushover curve reaches a plateau.

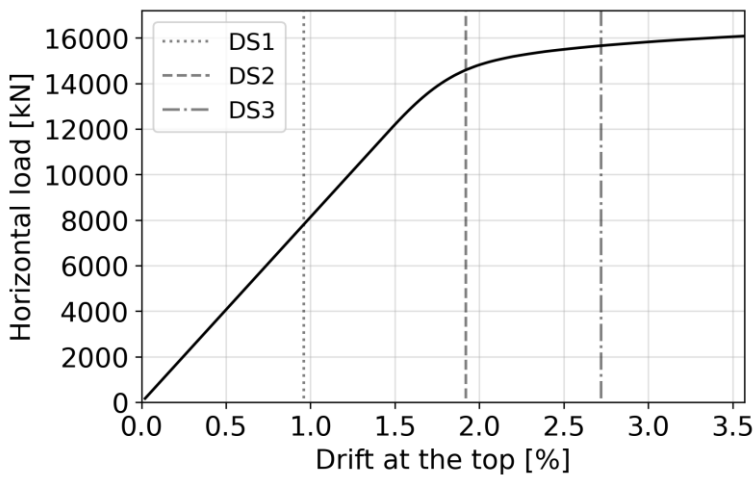

Fig. 3.1 Pushover curve of the wind turbine support structure.

3.5. Nonlinear response history analysis

The response time history of the OWT's support structure subjected to wave loading for each sea state considered is obtained by performing nonlinear dynamic analysis using the OpenSees software. As already mentioned, apart from material nonlinearity, the model developed accounts for geometric nonlinearity as well. The response of the structure is measured in terms of drift at the top of the tower. Static self-weight loads and wind loads are imposed on the tower for the duration of the dynamic analysis, the latter having the same orientation as the hydrodynamic loads originating from the uni-directional nonlinear irregular

wave. Rayleigh damping is used, while the damping ratio for the first two eigenmodes is considered to be 5%. The total duration of the dynamic analysis is 600 s.

The Newmark's method assuming average constant acceleration between time steps is implemented for performing the dynamic analyses. It is known that the accuracy of the method depends on the temporal discretization used. Two typical errors introduced by the method when using a high value for the time step are amplitude dissipation and period elongation. It is therefore important for the accuracy of the results that a low value for the time step of the analyses be used. On the other hand, given the total duration of each analysis, using low values for the time step would lead to them becoming computationally very demanding. It is therefore essential that the time step be kept as large as possible while still maintaining accuracy. To determine an appropriate value, a series of analyses were performed using different time steps ranging from 0.01 s to 0.5 s. Since the response histories obtained from analyses with time steps dt ≤0.05 s were found to converge, it is concluded that the a step equal to 0.05 s should be used.

3.6. Probability distribution of the structural response extreme values

Evaluation of the probability distribution of the extreme response values the support structure may exhibit due to the environmental loading is achieved by means of the Monte Carlo time simulation technique. It is noted that when using a small number of Monte Carlo simulations to determine the probability distributions of extreme responses, probabilities of exceedance with high decimal place accuracy cannot be estimated accurately. However, the aim of this study is to present a framework for producing the fragility of an OWT when subjected to increasingly intense sea states, and since larger number of simulations for each sea state would lead to excessive computer run-times, a total of 200 simulations were performed for each one.

The response time history record for each simulation is produced by performing dynamic analysis, as explained in Section 4.2, and each extreme response value is determined. All simulated extreme response values are then ranked from smallest to largest and the probability of each one being exceeded is calculated. An example of 200 extreme response values and their empirical cumulative probability distribution for a sea state characterized by an H_s = 17 m and a T_p = 15.49 s is presented in 0. The threshold values in terms of drift at the top of the tower corresponding to the three damage states considered are also depicted in the figure.

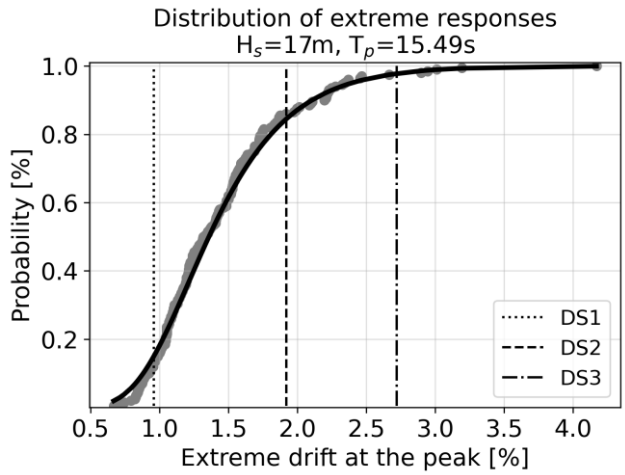

Fig. 3.2 Empirical distribution of the extreme responses of the support structure obtained by 200 Monte Carlo simulations for a sea state characterized by H_s = 17 m and T_p = 15.49 s.

The probability of exceedance for each damage state is estimated as the number of extreme response values surpassing the threshold drift values designated for a particular damage state over the total number of extreme responses simulated. For the example presented above the exceedance probabilities for DS_1, DS_2 and DS_3 are 88%, 14% and 3% respectively.

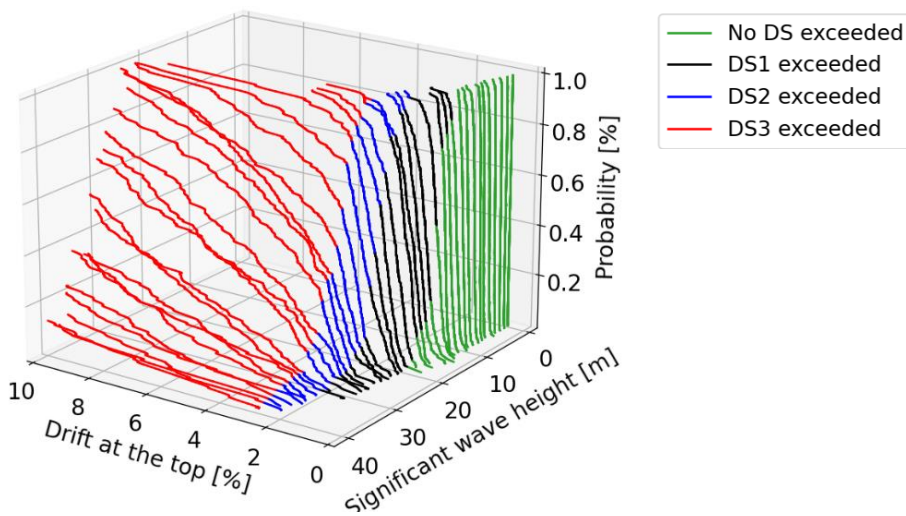

Fig. 3.3 Empirical distributions of the extreme responses for increasingly intense sea states.

The procedure for evaluating the probability distribution of the extreme responses is repeated for each of the 40 sea states considered. 0 presents the empirical distributions produced as a function of the significant wave height. As is observed, higher H_s values correspond to higher probabilities that larger drifts at the top would occur. In 0 the simulated extreme responses are color coded depending on whether a particular DS has been exceeded.

3.7. Fragility curves

The fragility of the monopile OWT as a function of the significant wave height is presented in 0. Apart from the wave loads, wind loads calculated using the 50-year mean wind speed are also exerted on the structure. The three curves depicted correspond to the damage states considered in this study, namely, 50% of the drift at the top at which yielding of the structure occurs, the yielding drift, and the drift at which the OWT is assumed to attain total damage and the pushover curve has reached a plateau.

It is apparent that sea states characterized by higher wave heights are associated with larger drifts at the top of the tower and with higher exceedance probabilities for each damage state. As shown in 0, the fragility curves produced indicate a 0% probability that any damage state will be exceeded for sea states characterized by an $H_s \leq 10$ m. However, it is likely that exceedance probabilities greater than 0% would be estimated if more simulations were conducted and results with higher decimal accuracy were produced.

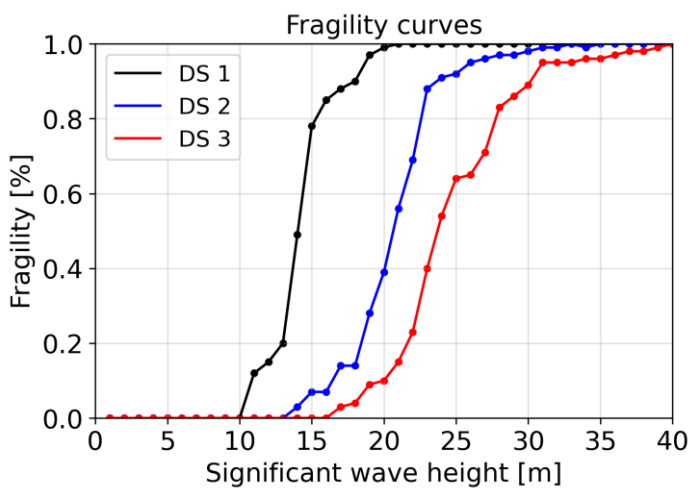

Fig. 3.4 Fragility curves of the monopile OWT support structure for the three damage limit states considered.

Regarding DS_1 it is found that there is 11% probability of it being exceeded for sea conditions characterized by an H_s of 11 m, while for H_s = 14 m the probability rises to 49%. As is expected similar probabilities that the other two damage states would be attained correspond to higher values of H_s. Specifically, it is found that DS_2 and DS_3 have 14% and 10% probability of exceedance for sea states characterized by an H_s of 17 m and 20 m, respectively. The 56% exceedance probability of DS_2 corresponds to an H_s value of 21 m, while for H_s = 24 m, the probability that DS_3 will be exceeded is 54%.

4. Conclusions

In this study, the effect of the significant wave height on the fragility of a monopile OWT support structure subjected to extreme environmental conditions present in SEM-REV, a location in the west coast of France, was studied. Nonlinear irregular waves were simulated to determine the hydrodynamic loading of the structure. A pushover analysis was performed and a curve depicting the nonlinear displacements at the top of the tower with increasing vertical loads was produced. Three damage limit states were defined with respect to which the fragility of the OWT was assessed. The first corresponds to 50% of the drift at the peak at which yielding of the structure occurs, the second corresponds to the yielding drift and the third to the drift at which the pushover curve reaches a plateau and the structure collapses. Sea states characterized by significant wave heights ranging from 1 to 40 m were considered. Nonlinear dynamic analyses were carried out to determine the extreme responses of the support structure in terms of drift at the top of the tower, when subjected to the wave induced hydrodynamic loads for each sea state taken into account. The empirical probability distribution of the extreme responses was estimated by employing the Monte Carlo simulation method.

This study represents a step forward by simulating nonlinear irregular waves to obtain the hydrodynamic loads originating from them while assessing the fragility of the monopile OWT. It was found that for sea states characterized by an H_s = 11 m, there is 11% probability that the DS_1 will be exceeded, while for a sea state characterized by an H_s = 14 m the probability rises to 49%. Yielding has 14% chance of occurring for a sea state characterized by an H_s = 17 m. For H_s = 21 m the yielding exceedance probability was found to be 56%. The probabilities that DS_3 will be exceeded for H_s = 20 m and H_s = 24 m are 10% and 54%, respectively.

Several simplifications and assumptions were made while conducting this study. Specifically, the monopile of the OWT was assumed to be rigidly fixed to the ground and the interaction between the structure and the soil was not taken into account. For simplicity, the imposed wind loads on the structure were considered to be static, while current loads were not taken into account. Additionally, a fairly small number of Monte Carlo simulations were run to deduce the empirical distributions of extreme responses, in order for excessive

computer run-times to be averted. Although the framework employed to derive the fragility curves in this study was not affected by these assumptions and simplifications, their final shape was. It is therefore suggested that refinements like accounting for the soil-structure interaction and for the current loads are made in future research efforts.

References

[1] Letcher, T.M., 2017. Wind energy engineering: A handbook for onshore and offshore wind turbines. Academic Press.

[2] Ruiz, R.V., 2020. Implementation and validation of dynamic wind turbine models for grid integration (Doctoral dissertation, Universidad de Castilla-La Mancha).

[3] REN21, 2022, Global Status Report, accessed September 2022, <https://www.ren21.net/wp-content/uploads/2019/05/GSR2021_Full_Report.pdf>.

[4] WindEurope, 24 February 2022, Wind energy in Europe: 2021 Statistics and the outlook for 2022-2026, accessed September 2022, <https://windeurope.org/intelligence-platform/product/wind-energy-in-europe-2021-statistics-and-the-outlook-for-2022-2026/>.

[5] Velarde, J., 2016. Design of monopile foundations to support the DTU 10 MW offshore wind turbine (Master's thesis, NTNU).

[6] Hübler, C.J., 2019. Efficient probabilistic analysis of offshore wind turbines based on time-domain simulations (Doctoral dissertation, Hannover: Institut für Statik und Dynamik, Leibniz Universität Hannover).

[7] Dodge, D.M., 2002. Illustrated History of Wind Power Development–20th Century Developments.

[8] Müller, G., Jentsch, M.F. and Stoddart, E., 2009. Vertical axis resistance type wind turbines for use in buildings. *Renewable Energy*, 34(5), pp.1407-1412.

[9] Islam, S.M., Nayar, C.V., Abu-Siada, A. and Hasan, M.M., 2018, Power Electronics for Renewable Energy Sources, Power Electronics Handbook, 4th Edition, Butterworth-Heinemann, Oxford, 783-827.

[10] Johnson, G.L., 1985. Wind energy systems (pp. 147-149). Englewood Cliffs, NJ: Prentice-Hall.

[11] Marie, D.G.J., LEBLANC VICKERS MAURICE SA, 1931. Turbine having its rotating shaft transverse to the flow of the current. U.S. Patent 1,835,018.

[12] Johannes, S.S., 1929. Rotor adapted to be driven by wind or flowing water. U.S. Patent 1,697,574.

[13] Winslow, A.R., 2017. Urban wind generation: comparing horizontal and vertical axis wind turbines at Clark University in Worcester, Massachusetts.

[14] Wuxi Flyt New Energy Technology Co.,Ltd., 16 June 2021, WIND TURBINE GENERATOR-NEW SOLUTION FOR FREE ENERGY POWER, accessed 25 September 2022, <https://www.flytpower.com/news/wind-turbine-generator-new-solution-for-free-energy-power/>

[15] Burton, T., Jenkins, N., Sharpe, D. and Bossanyi, E., 2011. Wind energy handbook. John Wiley & Sons.

[16] Zheng, C.W., Li, C.Y., Pan, J., Liu, M.Y. and Xia, L.L., 2016. An overview of global ocean wind energy resource evaluations. *Renewable and Sustainable Energy Reviews*, 53, pp.1240-1251.

[17] Kaldellis, J.K. and Kapsali, M., 2013. Shifting towards offshore wind energy—Recent activity and future development. *Energy policy*, 53, pp.136-148.

[18] Piasecka, I., Tomporowski, A., Flizikowski, J., Kruszelnicka, W., Kasner, R. and Mroziński, A., 2019. Life cycle analysis of ecological impacts of an offshore and a land-based wind power plant. *Applied Sciences*, 9(2), p.231.

[19] Syed Ahmad SZA, Abu Husain MK, Mohd Zaki NI, Mukhlas NA, Mat Soom E, Azman NU, Najafian G. 2021.Offshore Structural Reliability Assessment by Probabilistic Procedures—A Review. Journal of Marine Science and Engineering. 9(9):998.

[20] Mohd Zaki, N.I., Abu Husain, M.K. and Najafian, G., 2013, June. Comparison of extreme responses from wheeler and vertical stretching methods. In International Conference on Offshore Mechanics and Arctic Engineering (Vol. 55324, p. V02AT02A048). American Society of Mechanical Engineers.
[21] Mukhlas, N.A., Mohd Zaki, N.I., Abu Husain, M.K., Syed Ahmad, S.Z.A. and Najafian, G., 2022. Efficient derivation of extreme non-Gaussian stochastic structural response using finite-memory nonlinear system. Part 2: model validation. Ships and Offshore Structures, 17(6), pp.1209-1223.
[22] API. Recommended Practice for Planning, Designing and Constructing Fixed Offshore Platforms—Working Stress Design; American Petroleum Institute: Washington, DC, USA, 1993.
[23] Zaki, N.I.M., Husain, M.K.A. and Najafian, G., 2018. Comparison of Extreme Surface Elevation for Linear and Nonlinear Random Wave Theory for Offshore Structures. In MATEC Web of Conferences (Vol. 203, p. 01021). EDP Sciences.
[24] Agarwal, P., Manuel, L. 2011. Incorporating irregular nonlinear waves in coupled simulation and reliability studies of offshore wind turbines. Applied Ocean Research. 33(3): 215–227.
[25] Mirzadeh, J., Kimiaei, M., Cassidy, M.J. 2016. A Framework to Efficiently Calculate the Probability of Failure of Dynamically Sensitive Structures in A Random Sea. Ocean. Eng., 110: 215–226.
[26] Vestas Wind Systems A/S, 6 July 2009, 3.0 MW - an efficient way to more power, accessed November 2021, <https://arquivo.pt/wayback/20090706121351/http://www.vestas.com/en/wind-power-solutions/wind-turbines/3.0-mw>
[27] Li, L., Gao, Z. and Moan, T., 2013, June. Joint environmental data at five European offshore sites for design of combined wind and wave energy devices. In International Conference on Offshore Mechanics and Arctic Engineering (Vol. 55423, p. V008T09A006). American Society of Mechanical Engineers.
[28] McKenna, F., Fenves, G.L., Scott, M.H. and Jeremic, B., 2000. Open system for earthquake engineering simulation (OpenSees). Pacific Earthquake Engineering Research Center, University of California, Berkeley, CA.
[29] CEN, 1990. European Committee for Standardization, Eurocode 1: Basis of Design and Actions on Structures. Part 1: Basis of Design. – Part 1.4: General Actions – Wind Actions.
[30] Veritas, D.N., 2010. Recommended practice DNV-RP-C205: environmental conditions and environmental loads. DNV, Norway.
[31] Tucker, M.J., Challenor, P.G. and Carter, D.J.T., 1984. Numerical simulation of a random sea: a common error and its effect upon wave group statistics. Applied ocean research, 6(2), pp.118-122.
[32] Agarwal, P. and Manuel, L., 2008. Wave models for offshore wind turbines. In 46th AIAA Aerospace Sciences Meeting and Exhibit (p. 1336).
[33] International Electrotechnical Commission, 2009. Wind turbines: Part 3: Design requirements for offshore wind turbines
[34] Chakrabarti, S., 2005. Handbook of Offshore Engineering (2-volume set). Elsevier.
[35] Mitropoulou, Ch., Papadrakakis, M. 2011. Developing fragility curves based on neural network predictions, Engineering Structures, 33: 3409-3421.
[36] Cha, Y.J, Bai, J.W. 2016. Seismic fragility estimates of a moment-resisting frame building controlled by MR dampers using performance-based design, Eng Struct, 116: 192-202.
[37] Wu, T., Wang, L., Zhao, L., Fan, G., Wang, J., Yin, L., Zhang, S. and Liu, S., 2022. Seismic Fragility of a Multi-Frame Box-Girder Bridge Influenced by Seismic Excitation Angles and Column Height Layouts. Buildings, 12(3), p.387.
[38] Choi, E., DesRoches, R. and Nielson, B., 2004. Seismic fragility of typical bridges in moderate seismic zones. Engineering structures, 26(2), pp.187-199.
[39] Myers, A., Gupta, A., Ramirez, C. and Chioccarelli, E., 2012, September. Evaluation of the seismic vulnerability of tubular wind turbine towers. In Proceedings of the 15th world conference on earthquake engineering, Lisbon, Portugal (pp. 24-28).

[40] Kim, D.H., Lee, S.G. and Lee, I.K., 2014. Seismic fragility analysis of 5 MW offshore wind turbine. Renewable energy, 65, pp.250-256.
[41] Nuta, E., 2010. Seismic analysis of steel wind turbine towers in the Canadian environment. Toronto, ON, Canada: University of Toronto.
[42] Wilkie, D. and Galasso, C., 2020. A probabilistic framework for offshore wind turbine loss assessment. Renewable Energy, 147, pp.1772-1783.
[43] Wei, K., Arwade, S.R., Myers, A.T., Hallowell, S., Hajjar, J.F. and Hines, E.M., 2015. Performance levels and fragility for offshore wind turbine support structures during extreme events. In Structures Congress (pp. 1891-1902).
[44] Mardfekri, M. and Gardoni, P., 2013. Probabilistic demand models and fragility estimates for offshore wind turbine support structures. Engineering Structures, 52, pp.478-487.
[45] Zuo, H., Bi, K., Hao, H., Xin, Y., Li, J. and Li, C., 2020. Fragility analyses of offshore wind turbines subjected to aerodynamic and sea wave loadings. Renewable Energy, 160, pp.1269-1282.
[46] Yuan, C., Chen, J., Li, J. and Xu, Q., 2017. Fragility analysis of large-scale wind turbines under the combination of seismic and aerodynamic loads. Renewable Energy, 113, pp.1122-1134.